Proceedings of the ASME 2010 3rd Joint US-European Fluids Engineering Summer Meeting and 8th International Conference on Nanochannels, Microchannels, and Minichannels
FEDSM-ICNMM2010
August 1-5, 2010, Montreal, Canada

FEDSM-ICNMM2010-31104

EXPERIMENTAL AND NUMERICAL STUDY OF A PITCHING BLADE

M. R. Amiralaei
Department of Aerospace
Engineering, Ryerson University
Toronto, ON, Canada, M5B 2K3
mamirala@ryerson.ca

H. Alighanbari
Department of Aerospace
Engineering, Ryerson University
Toronto, ON, Canada, M5B 2K3
halighan@ryerson.ca

ABSTRACT

The objective of the present study is to investigate the effects of the reduced frequency on the aerodynamic characteristics of a three dimensional pitching blade. Experimental data are recorded at three sections of the blade model; tip, middle, and root sections at low and high turbulence intensities. A 2D numerical simulation is also conducted based on the Unsteady Reynolds Averaged Navier-Stokes (URANS) equations and Finite Volume Method (FVM) and the results are compared with those of the experimental observations. The results show that 2D numerical simulations are useful in obtaining the qualitative behavior of the flow field. Moreover, it is shown experimentally that the reduced frequency is of great importance to the flow physics. It affects the maximum lift coefficients, hysteresis loops, lift curve slopes, and angles at which stall occurs.

INTRODUCTION

The increasing demand for cost-competitive, environmentally-friendly, and renewable energy resources has raised a great attention to wind turbines. However, the inherent complexity of their unsteady aerodynamics makes it difficult to predict and analyze their aerodynamics and performance. Wind turbines operate in the lowest part of the earth boundary layer, and they are subjected to complicated effects such as environmental turbulence, directional and spatial variations in the wind shear, and oscillations. Indeed, "low turbulence intensity (T.I.)" and "steady wind" is an off-design condition for wind turbines [1]. Consequently, wind turbines operate almost always in an unsteady flow condition.

Since the blade loads and performance of a wind turbine are directly determined by the unsteady aerodynamic forces, an in depth knowledge of wind turbine flow characteristics and the effective parameters on its performance is of great importance to wind turbine designers [2].

Even though many of the aerodynamic phenomena occurring during the operation of these devices are known, the details of flow behavior are not still well understood [2], and various studies are being conducted to investigate these details.

Blade oscillations are among the unsteady conditions for wind turbines. These oscillations can be pitching, plunging, or flapping; though the pitching oscillations are more important. The reduced frequency, k, associated with these oscillations is an important factor in the flow behavior. The effects of reduced frequency on the corresponding aerodynamic forces and moments, flow separation, and hysteresis loops have been investigated by various researchers [3-9]. However, there is no report on the effect of turbulence intensities on the performance of a blade subjected to three dimensional unsteady flows [10]. Basically, information about flow phenomena associated with a three dimensional oscillating model in perturbed and unperturbed flow conditions is rare and more investigations are needed to fill the existing gap.

In the present study, the effects of k in low and high turbulence intensities on the lift and pressure coefficients of a 3D pitching blade are investigated experimentally. The study is performed at three sections of the model; tip, middle, and root sections. A 2D numerical simulation is also conducted based on the Unsteady Reynolds Averaged Navier-Stokes (URANS) equations and Finite Volume Method (FVM) and the results are compared with those of the experimental observations. The computations are performed in OpenFOAM [11].

NOMENCLATURE

c	=	airfoil chord-length
C_d	=	drag coefficient
C_l	=	lift coefficient
C_p	=	pressure coefficient
k	=	reduced frequency ($\pi fc/V_\infty$)
Re	=	Reynolds number

T.I. = turbulence intensity

EXPERIMENTAL FACILITY

All tests were conducted in a subsonic wind tunnel of closed return type having a total dimension of 3.8×6.5×18 meters. The tunnel had a closed square test section of 80×80×200 cm. Temperature in the test section is adjustable between 25 to 40 C^o and the Re is variable between 5.29×10^5 and 5.26×10^6 per meter. The maximum wind speed in the test section is 100m/s. The turbulence intensity in the test section is less than 0.1% when no grid is installed. A turbulence screen can be added at the beginning of the tunnel test section in order to have different inflow turbulence intensities.

The tests were conducted at Re = 0.42, 0.63, and 0.84×10^6. In this paper the results for Re = 0.84×10^6 are presented. The blade (Fig. 1) had a 25cm chord and a 60 cm span bounded by its root section to the tunnel wall through a splitter plate. Three sections were considered on the model at tip, middle, and root areas. Each section had 25 pressure holes connected to a differential pressure transducer. The oscillation system to produce harmonic pitching oscillations includes an inverter, an AC motor, and connecting arms.

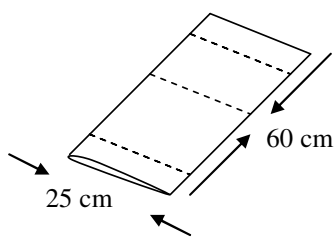

Fig. 1: Schematic of the pitching blade

NUMERICAL SIMULATION METHOD

The 2D Unsteady Reynolds-Averaged Navier-Stokes (URANS) equations govern the fluid flow of the 2D pitching blade in the desired Re range and the k-ε turbulence model is used for the closure problem.

O-type mesh is used for the simulations. At the inflow boundary, the velocity is set using Reynolds number and the pressure is restricted to the zero-gradient condition. At the outflow boundary, the pressure is set to the free stream value while the velocity is set to zero-gradient condition. The far-field boundary with symmetry boundary condition is set to 20c from the airfoil, in order to minimize the undesired effect on the airfoil's surrounding flow. The airfoil is set to no-slip boundary condition. The total number of cells was 100×10^3 and 2000 time steps were considered within one excitation period. This choice of grid size and temporal resolution was obtained after extensive grid and time sensitivity analyses. Fig. 1 shows the schematic of the airfoil, the computational domain, and the utilized boundary conditions.

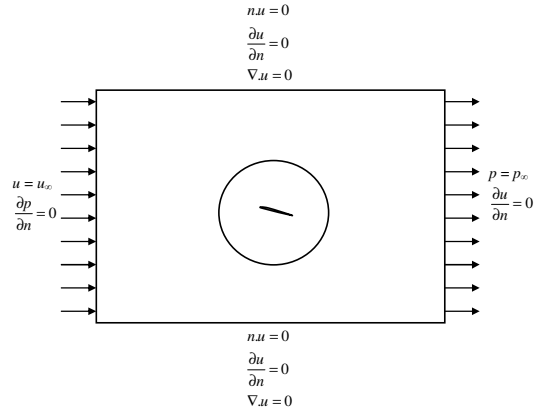

Fig. 2: Computational domain and the boundary conditions

The aerodynamics of a 2D airfoil is investigated based on FVM and URANS equations. The computations utilize a second order upwind scheme for convective, a second order central scheme for diffusive, and a second order Euler scheme for temporal terms. The resulting linear system of equations is treated with Preconditioned Conjugate Gradient (PCG) solvers, and the Pressure-Implicit with Splitting of Operators (PISO) algorithm is used for the pressure-velocity coupling. The computations are carried out in OpenFOAM [11]. The equation of motion is:

$$\alpha(t) = \alpha_0 + d\sin(2\pi ft) \tag{1}$$

where $\alpha(t)$ is the instantaneous angle of attack, α_0 is the mean angle of attack, d is the amplitude of pitching oscillations respectively, f is the frequency of pitching oscillation, and t is the physical time.

RESULTS AND DISCUSSION

The main purpose of the present study is to investigate the effects of k on the lift and pressure coefficients of a 3D blade under pitching oscillations. The real time pressures on the blade's surface are recorded at the blade tip, middle, and root sections, and the tests are conducted at low turbulence (unperturbed) and high turbulence (perturbed) conditions. A 2D numerical simulation is also performed to examine the 3D effects of on the lift coefficient. The simulation is performed for low-turbulence flow at k = 0.034. In this paper the data for a velocity of V_∞ = 60 m/s corresponding to Re = 84×10^6, α_0 = 10°, d = 5°, and k = 0.011, 0.017, and 0.034 are presented. Turbulence intensity was 0.08% for low-turbulence and 0.54% for high-turbulence conditions.

Effect of reduced frequency at the tip section

Figure 3 shows both static and dynamic lift coefficients at the tip section, when T.I. = 0.08. As illustrated, increasing k decreases $C_{l,\max}$. Moreover, as k increases, the angle of attack at

which $C_{l,\max}$ occurs remains almost constant as expected in the linear region of the static C_l. k also has significant effects on both hysteresis loops width and the lift curve slopes.

Figure 4 shows C_l versus α at T.I. = 0.54. It can be seen that k has similar effects on C_l as those observed in Fig. 3. The comparison between C_l of both T.I. = 0.08 and 0.54 is shown in Fig. 5 for k = 0.011 and 0.034. It is seen that the lift coefficients are higher at T.I. = 0.08 than those at T.I. = 0.54. Turbulence intensity does not have a noticeable effect on the lift curve slope and hysteresis width.

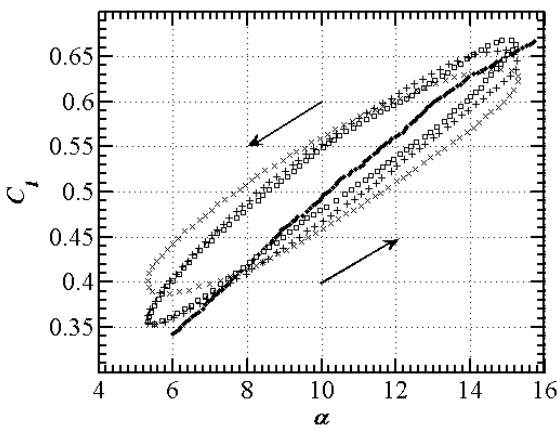

Fig. 3: C_l vs α for T.I. = 0.08 and k = 0.011 (□), k = 0.017 (+), k = 0.034 (×), k = 0 (*)

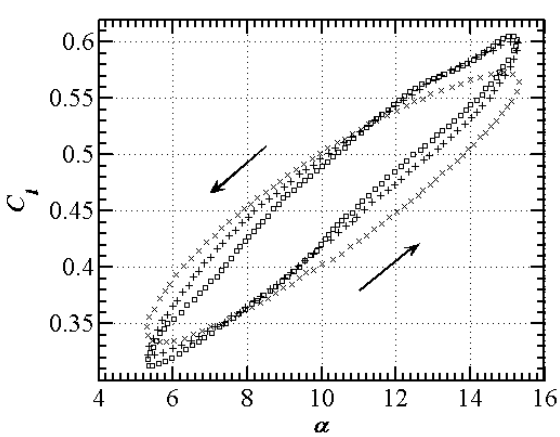

Fig. 4: C_l vs α for T.I. = 0.54 and k = 0.011 (□), k = 0.017 (+), k = 0.034 (×)

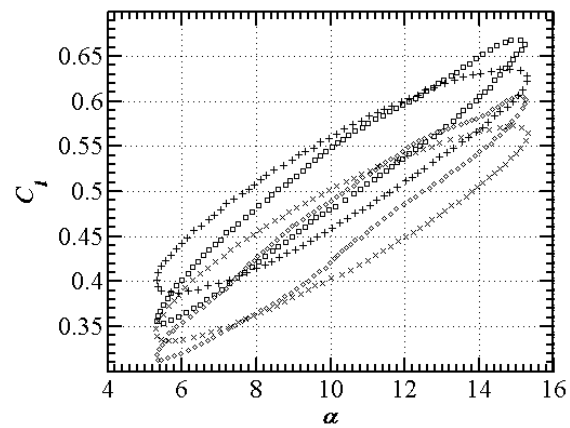

Fig. 5: Comparison between C_l vs α for k = 0.011 and T.I. = 0.08 (□), k = 0.011 and T.I. = 0.54 (◊), k = 0.034 and T.I. = 0.08 (+), k = 0.034 and T.I. = 0.54 (×)

Effect of reduced frequency at the middle section

Figure 6 shows C_l versus α for k = 0.011, 0.017, and 0.034 at the middle section of the blade when T.I. = 0.08. First, $C_{l,\max}$ decreases when k is changed from 0.011 to 0.017. Then, increasing k from 0.017 to 0.34 does not have any noticeable effect on $C_{l,\max}$. Moreover, the lift curve slope decreases and the hysteresis loops are broadened at higher reduced frequencies. Similar trend is observed in Fig. 7 when T.I. = 0.54. The comparison between these two flows, high and low turbulent flows, is shown in Fig. 8. As can be seen, high-turbulence intensity affects lift coefficients by delaying the occurrence of the so-called figure-eight phenomenon, after which the upstroke C_l is higher than that of the downstroke. This phenomenon is observed at k = 0.011 and 0.034 and T.I. = 0.08 and is delayed at k = 0.011 and T.I. = 0.54. Moreover, higher T.I. lowers the lift coefficient values, but it does not change the lift curve slopes.

Figure 9 shows the comparison between the 2D numerical simulation and the 3D experimental data. The calculated C_l from the computational study at upstroke is in close agreement with that of the experimental data. The discrepancy between the experimental and CFD simulation becomes larger after $\alpha \approx 14^o$. The experimental results show the occurrence of the figure-eight pattern which is not predicted by the numerical approach. The difference between the downstroke values of the two approaches (experimental and numerical) is bigger than that of the upstroke and becomes larger after $\alpha \approx 10^o$. This difference could be related to the existence of 3D vortices initiated from the tip and the root sections of the model. Despite the discrepancies between the results of the utilized solution methods, the 2D simulations are useful in determining the qualitative behavior of 3D model (at the middle section) and to investigate the important parameters to the aerodynamic characteristics.

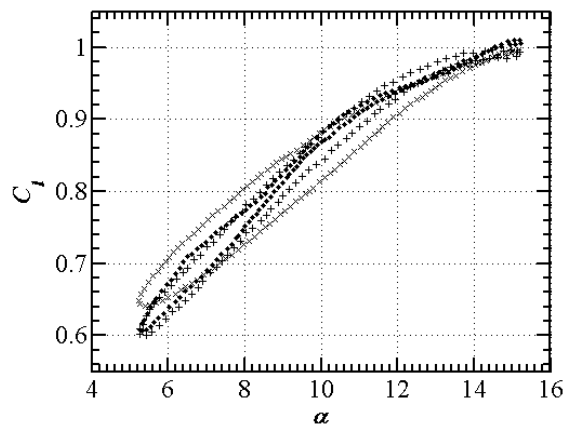

Fig. 6: C_l vs α for T.I. = 0.08 and k = 0.011 (*), k = 0.017 (+), k = 0.034 (×)

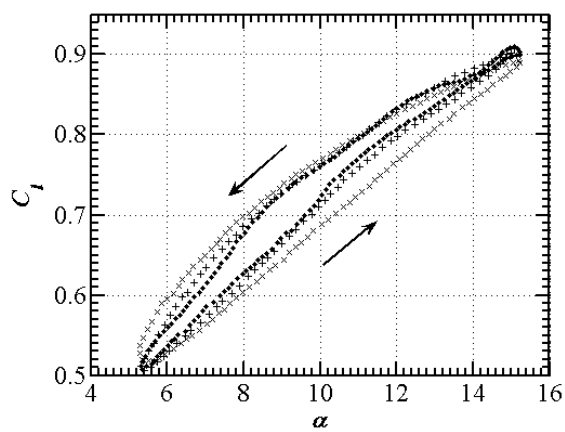

Fig. 7: C_l vs α for T.I. = 0.54 and k = 0.011 (*), k = 0.017 (+), k = 0.034 (×)

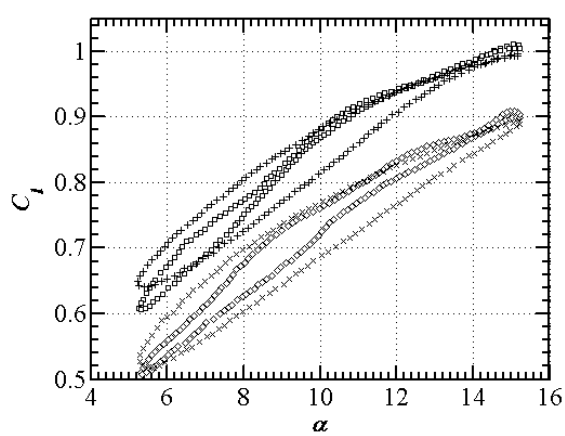

Fig. 8: Comparison between C_l vs α for k = 0.011 and T.I. = 0.08 (□), k = 0.011 and T.I. = 0.54 (◊), k = 0.034 and T.I. = 0.08 (+), k = 0.034 and T.I. = 0.54 (×)

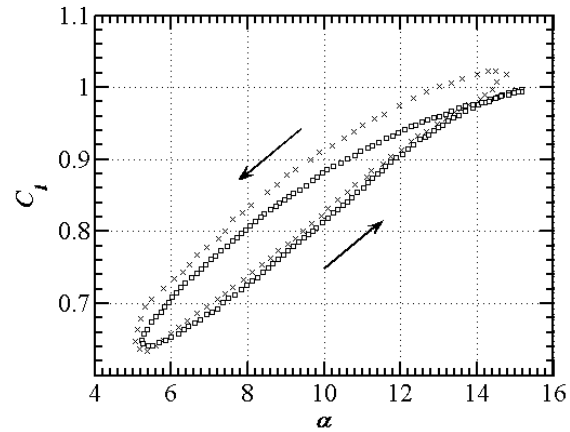

Fig. 9: C_l vs α at the middle section, experimental result (□), CFD (+), k = 0.034 and T.I. = 0.08

The time variation of pressure coefficients (C_p) versus the location of the pressure holes (x/c) are plotted at the middle section for k = 0.011, 0.017, and 0.034. Figure 10*a-c* shows C_p plots (carpet plots) at T.I. = 0.08. Both the suction (x/c = 0 to 1) and pressure (x/c = 1 to 2) sides of the model are shown.

It can be seen that increasing the reduced frequency does not affect the maximum pressure coefficient ($C_{p,\max}$), which remains almost constant ($C_{p,\max} \approx 2.7$) at the three examined reduced frequencies. Moreover, most of the C_p variation occurs in the first 50% span of the model ($0 < x/c < 0.5$). Figs. 11*a–c* show the pressure signatures at T.I. = 0.54. Similar effects as those seen in Fig. 10 are observed in Fig. 11, but the maximum pressure coefficient is less than that in the low-turbulence condition ($C_{p,\max} \approx 2.6$).

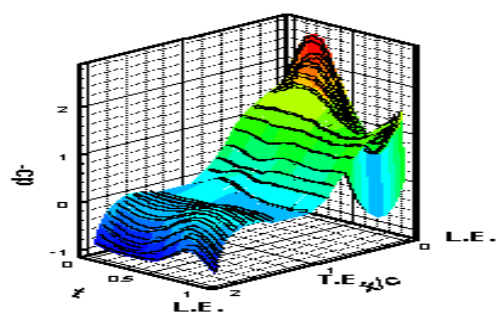

a) k = 0.011

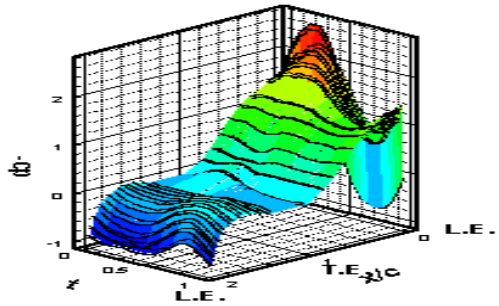

b) $k = 0.017$

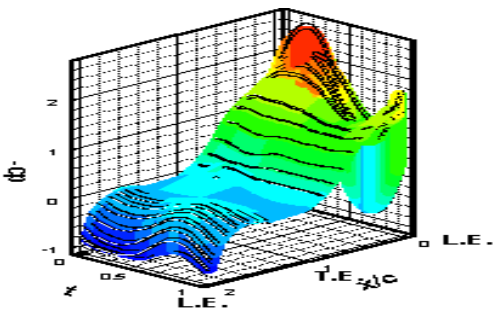

c) $k = 0.034$

Fig. 10: Time variation of C_p versus x/c at T.I. = 0.08

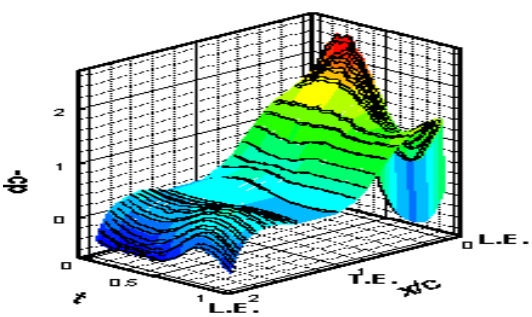

a) $k = 0.011$

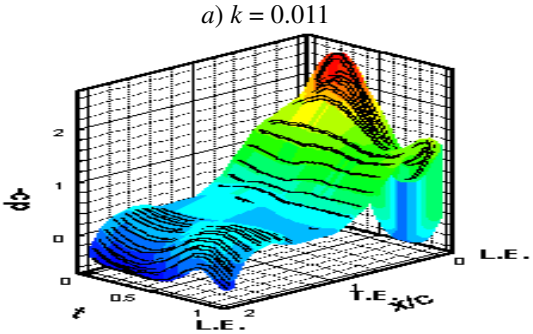

b) $k = 0.017$

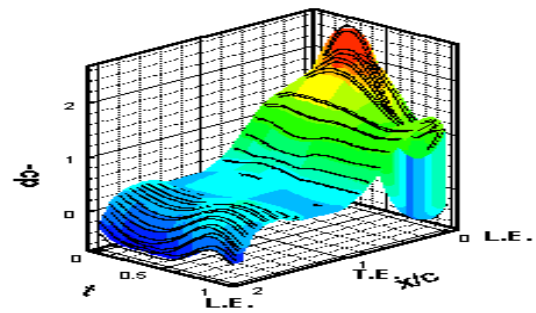

c) $k = 0.034$

Fig. 11: Time variation of C_p versus x/c at T.I. = 0.54

Effect of reduced frequency at the root section

C_l versus α for T.I. = 0.08 at the root section is shown in Fig. 12 .A figure-eight phenomenon is observed at $k = 0.011$ and $\alpha \approx 7^o$. At $\alpha \approx 10^o$, the lift coefficient faces a dynamic stall, characterized by the sudden decrease in C_l, which occurs earlier than the static stall angle of attack ($\alpha = 13^o$). Moreover, $C_{l,\max}$ at $k = 0.011$ is higher than the static $C_{l,\max}$, Fig. 12.

Increasing k lowers the negative slope after the stall at $k = 0.017$, hence a weaker stall exists at $k = 0.017$. As the reduced frequency is increased, the negative slope after the dynamic stall is lowered, showing the occurrence of a weaker stall. The angle of attack at which this stall occurs is the same as that of $k = 0.011$ ($\alpha \approx 10^o$); however, the location of the figure-eight phenomenon changes to $\alpha \approx 6^o$. Furthermore, increasing k form 0.011 to 0.017 decreases the lift curve slope, figure 12.

Increasing k from 0.017 to 0.034 diminishes the figure-eight phenomenon, but the location of the stall is delayed to a higher angle of attack ($\alpha \approx 12^o$). The lift curve slope after the stall remains the same as that of the previous reduced frequency ($k = 0.017$), Fig. 12. $C_{l,\max}$ is also approximately the same for both $k = 0.017$ and 0.034.

Figure 13 shows C_l versus α for T.I. = 0.54 at the root section. A weak dynamic stall is seen almost at the end of the motion at $k = 0.011$. The figure-eight phenomenon at $k = 0.017$ occurs at $\alpha \approx 13^o$, and its location is changed to $\alpha \approx 11^o$ for $k = 0.034$. In general, increasing k lowers the lift curve slopes.

Figure 14 shows a comparison between the high and low turbulent flow lift coefficients of the root section. It can be seen that in higher turbulent flow (T.I. = 0.54), the dynamic stall occurs at higher angles of attack, and the figure-eight phenomenon is delayed to higher angles. The width of the hysteresis loops is broadened at T.I. = 0.08, and the lift coefficient values are smaller at higher T.I.

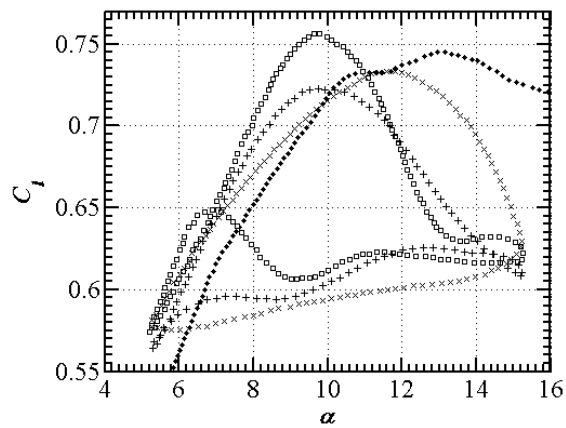

Fig. 12: C_l vs α for T.I. = 0.08,
k = 0.011 (□), k = 0.017 (+), k = 0.034 (×), k = 0 (*)

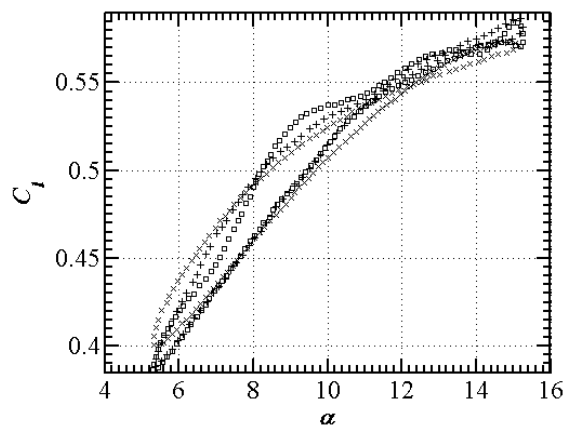

Fig. 13: C_l vs α for T.I. = 0.54,
k = 0.011 (□), k = 0.017 (+), k = 0.034 (×)

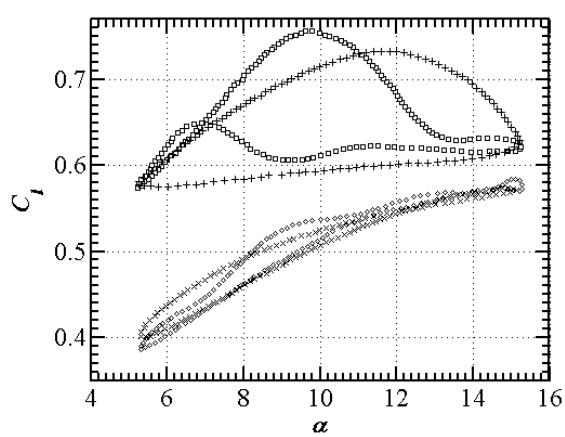

Fig. 14: Comparison between C_l vs α;
k = 0.011 and T.I. = 0.08 (□), k = 0.011 and T.I. = 0.54 (◊),
k = 0.034 and T.I. = 0.08 (+), k = 0.034 and T.I. = 0.54 (×)

CONCLUSION

An experimental study is conducted to investigate the effects of the reduced frequency on the force coefficients of a three dimensional blade under pitching motion. The instantaneous surface pressures are obtained at three different sections (tip, middle, and root) of the model and used to calculate the time variation of lift and pressure coefficients. 2D CFD study is also performed to obtain the lift coefficients at the middle section. The results show that 2D numerical simulations are useful in obtaining the qualitative behavior of the flow field. Computational results are in reasonably good agreement with the experimental data, and the discrepancy could be related to the spanwise vortices and the interaction of the tip and root vortical structures at the middle section. It is also shown experimentally that the reduced frequency is of great importance to the flow physics. It affects the maximum lift coefficients, hysteresis loops, and the lift curve slopes. It also changes the location of the dynamic stall and the figure-eight phenomenon.

Extensive wind tunnel tests were also conducted in high and low turbulence intensity flows to study the effects of reduced frequency on the pressure variation and aerodynamic performance of a section of the blade. Results show that reduced frequency is of great importance in the determination of the aerodynamic behavior quantitatively as well as qualitatively. It changes the maximum lift coefficient, lift curve slopes, and width of hysteresis loops. The so-called figure-eight phenomenon and dynamic stall are also affected. It is also observed that reduced frequency is of different importance to the flow regarding the turbulence intensity. It is also shown that increasing the turbulence intensity reduces the lift coefficient, delays the figure eight phenomenon thus separation, and weakens the dynamic stall intensity over the model.

ACKNOWLEDGEMENTS

The authors gratefully acknowledge the financial support of NSERC of Canada. The first author would also like to acknowledge the guidance given by Professor M. R. Soltani of Sharif University of Technology where most of the experimental work was performed.

REFERENCES

[1] Vermeer, K. J., Sqrensen, J. N., and Crespo, A., "Wind Turbine Wake Aerodynamics," *Progress in Aerospace Sciences*, Elsevier, 2003.

[2] Leishman, J. G., "Challenges in Modeling the Unsteady Aerodynamics of Wind Turbines," *21st ASME Wind Energy Symposium and 40th AIAA Aerospace sciences Meeting*, Reno, NV, 2002, pp. 2002-37.

[3] Hansen, A. C., and Butterfield, C. P., "Aerodynamics of Horizontal- Axis Wind Turbine," *Ann. Rev. of Fluid Mech.*, Vol. 25, 1993, pp.115-149.

[4] Mccroskey, W. J., "Unsteady Airfoils," Annual Rev. Fluid Mech. U.S. Army Aerodynamics Laboratory and NASA, 1982, pp. 285-309.

[5] Soltani, M. R., and Askari, F., "Roughness and Turbulence Effects on the Aerodynamic Efficiency of a Wind Turbine Blade Scetion," *Ankara International Aerospace Conference*, 2005, pp. 057.

[6] Huyer, S. A., Simms, D. A., and Robinson, M.C., "Unsteady Aerodynamics Associated with a Horizontal Axis Wind Turbine," *AIAA Journal*, Vol. 34, No. 7, 1996, pp. 1410-1419.

[7] Walker, J. M., Helin, H. E., and Chow, D. C., "Unsteady Surface Pressure Measurement on a Pitching Airfoil," AIAA Paper 85-0532, AIAA Shear Flow Control Conference, 1985.

[8] Swalwell K. E., Sheridan, J. and Melbourne, W. H., "The Effect of Turbulence Intensity on Performance of a NACA 4421 Airfoil Section," AIAA Paper 2004-0665, 2004.

[9] Soltani, M. R., and Seddighi, M., "The Effects of Reduced Frequency on Aerodynamic Performance of A Wind Turbine Blade," 14th International Conference of Mechanical Engineering, Iran, 2006.

[10] Swalwell, K. E., Sheridan, J., and Melbourne, W. H., "The Effect of Turbulence Intensity on Stall of the NACA 0021 Aerofoil," *14th Australasian Fluid Mechanics Conference,* Adelaide University, Australia, Adelaide, Dec. 2001, pp. 10-14.

[11] OpenFOAM, the Open Source CFD Toolbox, User Guide, version 1.4.1, August 2007.